



Short Communication

MEMS implementation of axial and follower end forces

Abhyudai Singh^a, Ranjan Mukherjee^{a,*}, Kimberly Turner^b, Steven Shaw^a^a*Department of Mechanical Engineering, Michigan State University, 2555 Engineering Building,
East Lansing, MI 48824-1226, USA*^b*Department of Mechanical Engineering, University of California, Santa Barbara, CA 93106, USA*

Received 27 October 2004; received in revised form 23 November 2004; accepted 10 December 2004

Abstract

Although it is challenging to implement follower forces in macroscale laboratory experiments, they can be implemented fairly easily in MEMS devices. This paper discusses the implementation of follower and axial end forces in a beam-type MEMS resonator for the application of resonant frequency tuning.

© 2005 Elsevier Ltd. All rights reserved.

1. Introduction

The transverse vibrations of slender beams subjected to constant amplitude end loads is a classical, well-understood subject. While axial end loads can lead to buckling, follower forces are a standard means of introducing flutter [1]. Other types of end loads are also possible, for example, those that are combinations of follower and axial loads [2], as well as variable-orientation bucking-type loads [3]. It is quite simple to experimentally apply axial forces on beams by making use of dead loads, but it is quite challenging to realize follower forces in the laboratory. To the authors knowledge, the only experimental implementations of follower forces make use of a fluid stream that is ejected from a nozzle fixed to the free end of a cantilever beam [4]. The convection of fluid along the beam, however, adds a term to the equation of motion [5], and leads to a situation that is not the textbook version of a follower force. In this paper we show that follower

*Corresponding author.

E-mail address: mukherji@egr.msu.edu (R. Mukherjee).

forces, as well as axial forces, can be easily implemented in MEMS, and these end loads provide the scope for performance enhancement of certain MEMS devices.

It is known that axial and follower end loads affect transverse vibration natural frequencies of a beam. In fact, tensile (compressive) axial loads increase (decrease) all the natural frequencies of a beam, while tensile (compressive) follower forces decrease (increase) the frequency of the fundamental mode of the beam; the same effect is seen for all odd-numbered modes while the opposite effect occurs for the second and all even-numbered modes [1]. Of course, these trends are valid so long as the axial and follower end loads remain below their buckling and flutter thresholds, respectively.

In this short communication we describe a new method for achieving both axial and follower forces on a microscale cantilever beam. This has significant potential for frequency tuning of microbeams, which are used in a number of current and proposed applications, including filters [6], sensors [7,8], atomic force microscopes [9], and high-density data storage devices [10]. In these applications, variability in the resonant frequency of a beam can arise from a number of sources, such as manufacturing tolerances, thermal effects, etc., and one must typically employ some type of feedback to maintain the natural frequency at a fixed value. One means of doing so is by providing end loads on the beam. In the approach described here, these loads are achieved using electrostatic forces that act near the free end of the beam through specially designed comb fingers. These combs are arranged so that the orientation of the applied force can remain aligned with the undeformed neutral axis of the beam, or can move with the beam such that the force remains parallel to the slope at the free end of the beam. In addition, by varying the spacing between the comb fingers on the beam and those fixed to ground, one can create either tensile or compressive axial and/or follower forces.

We begin with a brief review of the dynamics of a slender cantilever beam with axial and follower forces applied to the free end, emphasizing the effects that these loads have on the fundamental natural frequency of the beam. We then describe the proposed means of realizing these forces in a microbeam, and provide a specific design that is capable of achieving frequency tuning in the range of 20% without experiencing buckling or flutter. Several devices based on this basic design are currently being prepared for fabrication and testing.

2. Mechanics of a beam with end forces

Consider a uniform cantilever beam that has both a follower force F and an axial end load P applied to its free end. A dimensionless version of this system is shown in Fig. 1. If E denotes the

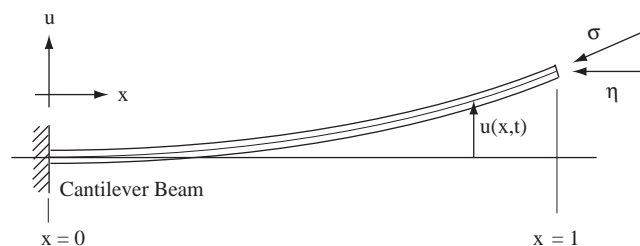


Fig. 1. A cantilever beam with axial and follower end loads.

Young's modulus, I the second area moment, ρ the mass density, and A the cross-sectional area of the beam, then with the usual assumption of the elementary theory of bending, the normalized equation of small oscillations of the beam is

$$\frac{\partial^4 u(x, t)}{\partial x^4} + (\sigma + \eta) \frac{\partial^2 u(x, t)}{\partial x^2} + \frac{\partial^2 u(x, t)}{\partial t^2} = 0, \quad (1)$$

where $u(x, t)$ is the transverse deflection of the beam normalized by the beam length L and measured such that $x = 0$ is the fixed end. Time has been rescaled by the characteristic frequency $\sqrt{EI/mL^4}$ and dimensionless load parameters are given by $\sigma = Fl^2/EI$ and $\eta = Pl^2/EI$. The boundary conditions can be written as

$$u(x, t)|_{x=0} = 0, \quad \left. \frac{\partial u(x, t)}{\partial x} \right|_{x=0} = 0, \quad \left. \frac{\partial^2 u(x, t)}{\partial x^2} \right|_{x=1} = 0, \quad \left[\left. \frac{\partial^3 u(x, t)}{\partial x^3} \right|_{x=1} + \eta \left. \frac{\partial u(x, t)}{\partial x} \right|_{x=1} \right] = 0. \quad (2)$$

Considering a separation of variable solution $u(x, t) = Y(x)Q(t)$ for Eq. (1) yields

$$\frac{Y''''}{Y} + (\sigma + \eta) \frac{Y''}{Y} = -\frac{\ddot{Q}}{Q} = \omega^2, \quad (3)$$

where prime and dot denote derivatives with respect to the spatial variable x , and the temporal variable t , respectively. From Eqs. (3) and (2), we have

$$Y'''' + (\sigma + \eta) Y'' - \omega^2 Y = 0 \quad (4)$$

and the boundary conditions

$$Y(0) = 0, \quad Y'(0) = 0, \quad Y''(1) = 0, \quad Y'''(1) + \eta Y'(1) = 0. \quad (5)$$

If we assume a spatial solution of the type $Y(x) = \exp(\lambda x)$, we get

$$\lambda^4 + (\sigma + \eta) \lambda^2 - \omega^2 = 0 \quad (6)$$

which yields

$$Y(x) = A \cosh(\lambda_1 x) + B \sinh(\lambda_1 x) + C \cos(\lambda_2 x) + D \sin(\lambda_2 x), \quad (7)$$

where

$$\lambda_1 = \sqrt{-\left(\frac{\sigma + \eta}{2}\right) + \sqrt{\left\{\frac{\sigma + \eta}{2}\right\}^2 + \omega^2}}, \quad \lambda_2 = \sqrt{\left(\frac{\sigma + \eta}{2}\right) + \sqrt{\left\{\frac{\sigma + \eta}{2}\right\}^2 + \omega^2}}. \quad (8)$$

The boundary conditions (5) can be used to numerically solve for the natural frequencies of the beam for different values of the follower force, σ , and axial force, η . Of particular interest to us, is the variation in the natural frequencies of the beam with variation in the magnitude of the follower force when the axial force is zero, and variation in the natural frequencies of the beam with variation in the magnitude of the axial force when the follower force is zero. Fig. 2(a) shows the first two natural frequencies of the beam as a function of the axial end load for zero follower force. This indicates the decreasing nature of the natural frequencies as η increases, and shows the end load at which the beam buckles to be $\eta_{cr} = 2.48$. Fig. 2(b) shows the first two natural frequencies as a function of the follower force for zero axial force. Note that as the follower force increases the first modal frequency increases while the second modal frequency decreases. These

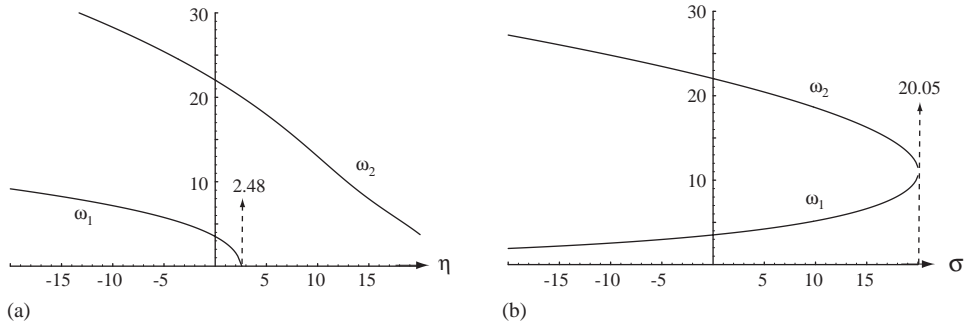


Fig. 2. Variation in the first two natural frequencies of the cantilever beam with (a) variation in axial force, for zero follower force, and (b) variation in follower force, for zero axial force.

two frequencies merge, resulting in flutter instability, at a critical value of the follower force given by $\sigma_{cr} = 20.05$. Note that one has a significantly larger working range for a compressive follower force as compared to a compressive axial end load. It is also clear from the plots that the slope of stiffness variation is steeper for the axial force as compared to the follower force, about zero nominal values.

One way to avoid buckling and flutter instability is to work with tensile axial and follower forces. From the plots in Fig. 2, it is clear that a tensile axial force will increase the resonant frequency of the beam whereas a tensile follower force will decrease the resonant frequency. Thus, double sided tuning, i.e. both increase and decrease of natural frequency, can be achieved with a large range of frequency variation. In the next section we present the design of a MEMS resonator with double-sided tuning capability.

3. Mechanical design of resonator

Consider the cantilever beam in Fig. 3(a) with two arc-shaped comb fingers. Each of the two fingers subtend angle α at the base of the beam and remain parallel to the fixed elements A and B , respectively. The fixed elements are located symmetrically with respect to the beam in the unperturbed state, and β denotes the angle of no overlap between the fingers and the fixed elements. The perturbed state is shown in Fig. 3(b) for small angular deflection of the beam, θ . In this state, the angular overlap between the fingers and the fixed elements A and B are $(\alpha - \beta + \theta)$ and $(\alpha - \beta - \theta)$, respectively. If F_A and F_B denote the electrostatic forces applied on the fingers by the fixed elements A and B , respectively, then the resultant of these forces have the following x and y components:

$$F_x = F_A \cos\left(\frac{\alpha + \beta + \theta}{2}\right) + F_B \cos\left(\frac{\alpha + \beta - \theta}{2}\right) = p \cos(\theta/2) - q \sin(\theta/2), \quad (9)$$

$$F_y = F_A \sin\left(\frac{\alpha + \beta + \theta}{2}\right) - F_B \sin\left(\frac{\alpha + \beta - \theta}{2}\right) = p \sin(\theta/2) + q \cos(\theta/2), \quad (10)$$

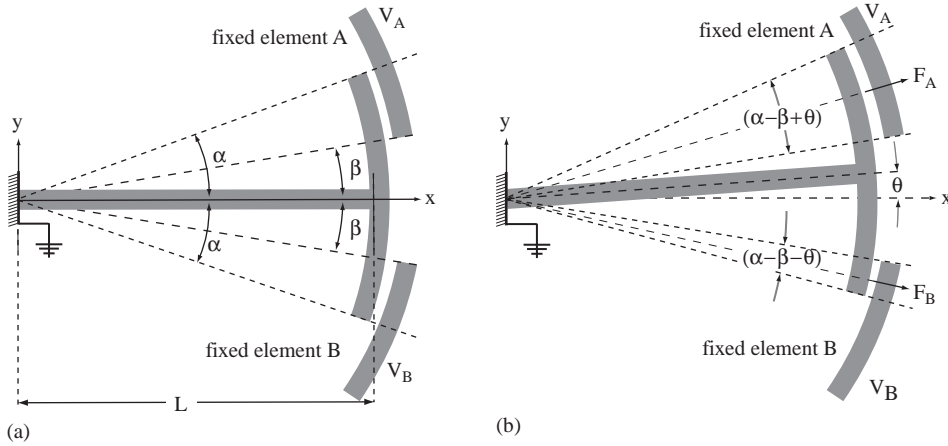


Fig. 3. A cantilever beam with two arc-shaped comb fingers in its (a) unperturbed state and (b) perturbed state. The fixed elements A and B are configured to apply tensile end forces.

where

$$p \triangleq (F_A + F_B) \cos \frac{(\alpha + \beta)}{2}, \quad q \triangleq (F_A - F_B) \sin \frac{(\alpha + \beta)}{2}.$$

If the resultant force subtends angle ψ with the x -axis, then ψ can be expressed as

$$\tan \psi = \frac{p \sin(\theta/2) + q \cos(\theta/2)}{p \cos(\theta/2) - q \sin(\theta/2)}.$$

The resultant force will be a follower force if $\psi = \theta$, and an axial force if $\psi = 0$. It can be easily shown that

$$\psi = \begin{cases} \theta & \text{if } F_A = K \sin[(\alpha + \beta + \theta)/2] \text{ and } F_B = K \sin[(\alpha + \beta - \theta)/2], \\ 0 & \text{if } F_A = K \sin[(\alpha + \beta - \theta)/2] \text{ and } F_B = K \sin[(\alpha + \beta + \theta)/2], \end{cases} \quad (11)$$

where K is any constant. Furthermore, for the choice of F_A and F_B in Eq. (11), the magnitudes of the follower and axial forces are constant and equal to $K \sin(\alpha + \beta)$. From electrostatic principles, the forces F_A and F_B are also given by the relations

$$F_A = \frac{\varepsilon_0}{2g^2} h V_A^2 L(\alpha - \beta + \theta), \quad F_B = \frac{\varepsilon_0}{2g^2} h V_B^2 L(\alpha - \beta - \theta), \quad (12)$$

where ε_0 is the electrostatic permittivity of vacuum, g is the radial gap between the comb fingers and fixed elements, h is the height of the resonator, L is the length of the beam, and V_A and V_B are the voltages applied between the comb fingers and the fixed elements A and B , respectively. Therefore, using Eqs. (11) and (12), V_A and V_B can be chosen appropriately (as functions of θ) to generate follower and axial end loads.

Based on this idea, we now provide a schematic of a resonator whose first resonant frequency can be tuned up or down through the application of axial and follower end forces. The resonator, shown in Fig. 4, has a set of anterior combs for the application of the end force (axial or follower)

and an additional set of lateral combs for actuation and sensing. The actuator combs will be used to provide sinusoidal excitation for resonance whereas the sensor combs will be used to measure the deflection of the beam in real-time. Although the deflection of the beam will remain small, all curved elements are designed by taking the radius of curvature of the beam (corresponding to the first mode shape) into consideration. This ensures that the gaps between the fixed and moving elements remain constant and prevents potential malfunctioning due to varying gap or mechanical contact.

4. Numerical simulation

Consider the MEMS resonator in Fig. 4 with the following specific dimensions and material property:

$$\alpha = 16^\circ, \quad \beta = 8^\circ, \quad h = 30 \mu\text{m}, \quad g = 2 \mu\text{m}, \quad E = 170 \times 10^9 \text{ Pa}. \quad (13)$$

Using a lumped-mass model of the fingers and the method of assumed modes, the first natural frequency was found to be approximately 7.5 kHz. To realize a follower force, voltages V_A and

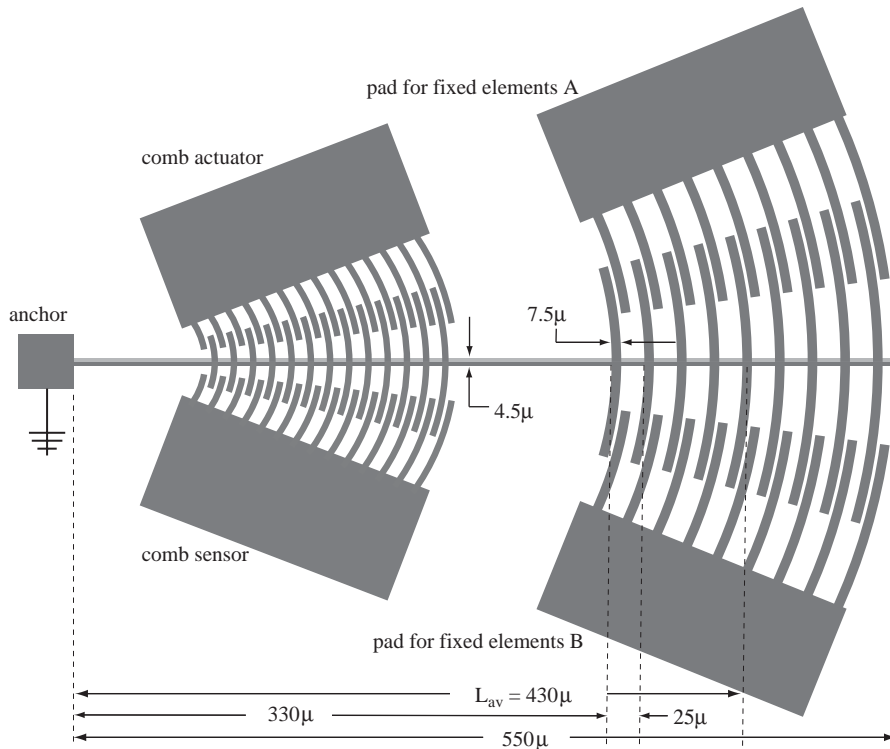


Fig. 4. Schematic of a MEMS resonator.

V_B were chosen as

$$V_A = V_0 \sqrt{\frac{(\alpha - \beta) \sin[(\alpha + \beta + \theta)/2]}{(\alpha - \beta + \theta) \sin[(\alpha + \beta)/2]}}, \quad V_B = V_0 \sqrt{\frac{(\alpha - \beta) \sin[(\alpha + \beta - \theta)/2]}{(\alpha - \beta - \theta) \sin[(\alpha + \beta)/2]}}. \quad (14a)$$

For an axial force, the voltages were chosen as

$$V_A = V_0 \sqrt{\frac{(\alpha - \beta) \sin[(\alpha + \beta - \theta)/2]}{(\alpha - \beta + \theta) \sin[(\alpha + \beta)/2]}}, \quad V_B = V_0 \sqrt{\frac{(\alpha - \beta) \sin[(\alpha + \beta + \theta)/2]}{(\alpha - \beta - \theta) \sin[(\alpha + \beta)/2]}}. \quad (14b)$$

It is clear from Eq. (14) that $V_A = V_B = V_0$ when $\theta = 0$. Furthermore, from Eqs. (11) and (12), it can be seen that for these choice of voltages,

$$K = \frac{\varepsilon_0 h V_0^2 n L_{av} (\alpha - \beta)}{2g^2 \sin[(\alpha + \beta)/2]}, \quad (15)$$

where $n = 9$ is the number of anterior fingers for application of end force, and $L_{av} = 430 \mu\text{m}$ is the average distance of the anterior fingers from the anchor. With this value of K and using $V_0 = 70 \text{ V}$, non-dimensional follower and axial forces with

$$\sigma = \eta = -\frac{K \sin(\alpha + \beta) L_{av}^2}{EI} \approx -1 \quad (16)$$

can be realized. From the analysis in Section 2, it can be seen that while $\sigma = -1$ decreases the first natural frequency by 425 Hz, $\eta = -1$ increases the natural frequency by 1.1 kHz. Thus, bi-directional frequency tuning with a range of approximately 1.5 kHz (20%) can be achieved through voltage adjustments.

Acknowledgements

The authors gratefully acknowledge the support provided by the Air Force Office of Scientific Research, Contract AFOSR FA 9550-04-1-0069, in carrying out this research.

References

- [1] V.V. Bolotin, *Nonconservative Problems of the Theory of Elastic Stability*, Pergamon Press, New York, 1963.
- [2] Q.H. Zuo, H.L. Schreyer, Flutter and divergence instability of nonconservative beams and plates, *International Journal of Solids and Structures* 33 (9) (1996) 1355–1367.
- [3] S. Nudehi, R. Mukherjee, S.W. Shaw, Vibration suppression in a cantilever beam using an end force, *ASME International Mechanical Engineering Congress and Exposition*, Anaheim, CA, 2004.
- [4] G. Herrmann, Dynamics and stability of mechanical systems with follower forces, Nasa Contractor Report, NASA CR-1782, 1971.
- [5] A.K. Bajaj, P.R. Sethna, Flow induced bifurcations to three-dimensional oscillatory motions in continuous tubes, *SIAM Journal of Applied Mathematics* 44 (1985) 270–286.
- [6] B. Piekarski, D. DeVoe, M. Dubey, R. Kaul, J. Conrad, R. Zeto, Surface micromachined piezoelectric resonant beam filters, *Sensors and Actuators A: Physical* 91 (3) (2001) 313–320.

- [7] B. Charlot, F. Parrain, N. Galy, S. Basrour, B. Courtois, A sweeping mode integrated fingerprint sensor with 256 tactile microbeams, *Journal of Microelectromechanical Systems* 13 (4) (2004) 636–644.
- [8] M. Yue, H. Lin, D.E. Dedrick, S. Satyanarayana, A. Majumdar, A.S. Bedekar, J.W. Jenkins, S. Sundaram, A 2-D microcantilever array for multiplexed biomolecular analysis, *Journal of Microelectromechanical Systems* 13 (2) (2004) 290–299.
- [9] S.I. Lee, S.W. Howell, A. Raman, R. Reifenberger, Nonlinear dynamics of microcantilevers in tapping mode atomic force microscopy: a comparison between theory and experiments, *Physics Review B* 66 (2002).
- [10] P. Vettiger, G. Coross, M. Despont, U. Drechsler, U. Durig, B. Gotsmann, W. Haberle, M.A. Lantz, H.E. Rothuizen, R. Stutz, G.K. Binnig, The millipede-nanotechnology entering data storage, *IEEE Transactions on Nanotechnology* 1 (1) (2002) 39–55.